Master Thesis
TVVR 15/5014

CFD MODELLING OF DAM SPILLWAY AERATOR

Raphaël Damiron

Division of Water Resources Engineering
Department of Building and Environmental Technology
Lund University

CFD MODELLING OF DAM SPILLWAY AERATOR

By:
Raphaël Damiron

Master Thesis

Division of Water Resources Engineering
Department of Building & Environmental Technology
Lund University
Box 118
221 00 Lund, Sweden

Water Resources Engineering
TVVR-15/5014
ISSN 1101-9824

Lund 2015
www.tvrl.lth.se

Master Thesis
Division of Water Resources Engineering
Department of Building & Environmental Technology
Lund University

English title:	CFD modelling of dam spillway aerator
Author(s):	Raphaël Damiron
Supervisor:	Magnus Larson James Yang
Examiner:	Rolf Larsson
Language	English
Year:	2015
Keywords:	<spillway; aerator; CFD;VOF; 3D flow>

LUND UNIVERSITY

Abstract

Lunds Tekniska Högskola
Department of Building and Environmental Technology

Master of Science Thesis

CFD MODELLING OF DAM SPILLWAY AERATOR

by Raphaël DAMIRON

The purposes of this master thesis are the simulation of the aerator air flow driven by the spillway water flow in the Bergeforsen dam and the behavior of the flow in the stilling basin. Aerators are employed to supply air at critical locations in the flow where low pressure and cavitation may occur in order to protect the structure. The simulations were carried out, first in 2D and then in 3D, with the software FLUENT/GAMBIT describing the spillway and the stilling basin. Results were mainly concentrate on the interface between phases, air entrainment but also velocity and pressure of the flow. Limited data from laboratory experiments were available; however, their usefulness might be limited due to scale effects occurring in such two-phase flow problems.

Acknowledgements

This work was carried out during my time as a student at the Faculty of Engineering, Lund University. I would like to thank all persons who supported me in Lund and contributed to the achievement of this master thesis, in particular:

Thank you to Prof. Magnus Larson for introducing and supervising this project, for his interest and contribution using his practical experience.

Many thanks to Prof. James Yang from Vattenfall who initiated the project and assist me with the help of his Phd. student: Penghua Teng.

I am grateful to Ali Al Sam from the Division of Fluid Mechanics who took on his time to help me with the simulation.

Contents

Symbols

a	Local speed of sound
C_a	Mean air concentration of developed aeration
d_0	Depth of flow at the beginning of the ramp
e_o	Total energy
k	Turbulent Kinetic Energy (TKE) per unit mass
$\dot{m}_{\mathrm{qp}}$	Mass transfer from phase q to phase p
$\dot{m}_{\mathrm{pq}}$	Mass transfer from phase p to phase q
M_t	Turbulent Mach number
$n; n+1$	Time step
p	pressure intensity
p_0	Local pressure
p_v	Vapor pressure of water
P_k	Production of turbulent kinetic energy due to the mean velocity gradients
P_b	Production of turbulence kinetic energy due to buoyancy
q_a	Unit discharge of air
q_w	Unit discharge of water
S_k	User-defined source terms of k
S_ϵ	User-defined source terms of ϵ
S_{ij}^*	Traceless viscous strain-rate tensor component
S_{α_q}	User-defined mass source for each phase
t	Time
t_r	Ramp height
t_s	Offset/duct height
u_i	Velocity magnitude
u_i'	Fluctuating component of velocity magnitude
$U_i, \bar{u_i}$	Average flow velocity
V_f	Volume flux through a face based on normal velocity
V	Volume of cell
X_i	Horizontal distance from end of ramp to jet impact location
X_n	Horizontal distance from end of ramp to centerline of jet at impact location

Y_i	Elevation at impact point
Y_n	Elevation of centerline of jet at impact point
Y_M	Contribution of the fluctuating dilatation to ϵ

α	Ramp angle
α_q	Volume fraction of a fluid in a cell
β	Air entrainment coefficient
$\beta_{Buoyancy}$	Coefficient of thermal expansion
δ_{ij}	Kronecker delta
ϵ	Turbulence dissipation rate per unit mass
σ	Cavitation number (index)
θ	Spillway slope
μ	Dynamic viscosity
μ_t	Eddy/Turbulent viscosity
ρ	Density
τ_{ij}	Viscous stress tensor component

Constants

k - ϵ Model Constants	$C_{1\epsilon} = 1.44$
	$C_2 = 1.90$
	$C_{3\epsilon} = -0.33$
Turbulent Prandtl numbers	$\sigma_k = 1.00$
	$\sigma_\epsilon = 1.20$

Abbreviations

CFD	**C**omputational **F**luid **D**ynamics
RANS	**R**eynolds-**A**veraged **N**avier-**S**tokes
VOF	**V**olume **O**f **F**luid

Chapter 1

Introduction

1.1 Project description

Spillways and chutes are important hydraulic structures for dam safety. They release floods so that the water does not overtop, damage or in the worst scenario destroy the dam. Except when the reservoir approach the full retention level, water does not normally flow over a spillway as it squandered potential energy. Due to the expect change in climate, several hydropower plants in Sweden are being revised to respect the new design flood guideline which expect an increase in the annual river discharge. The Bergeforsen dam, located at the Indalslven river mouth in Sweden is one of the dam concerned by this dam-safety upgrade. A new gated spillway has been build in addition to the already existing one in order to increase the total discharge capacity.

Due to the high velocities coupled with low pressure, cavitation may occur on the chute bottom provoking major damage and endanger the spillway stability. To protect the hydraulic structure, an aerator was built to add air in the flow. It is well known that extremely small quantities of air spread through water will significantly reduce the risk for cavitation to damage a surface.

1.2 Objectives

The objective of this thesis is to determine the air flow driven by the spillway flow and the behavior of the flow in the stilling basin. Although aerators have been investing during the past 50 years, the entrainment at the aerator and detrainment further downstream are still not fully understood with laboratory instruments. CFD modeling could help to understand the functioning of the aerator, which is essential for the safe operation of the

new spillway. It is expected to clarify such issues as air demand as a function of spillway discharge, pressure condition and air transport in the flow. Different discharge of the flow through the spillway considering a fixed downstream water level are going to be studied in two and three dimensions (see Table 1.1). The third dimensions is crucial to modeled the geometry of the spillway which is not projectable in two dimensions without simplifications on the aerator. It will also permit to model accurately the anisotropic flow behavior in the basin which is fully turbulent and by definition three-dimensional. However the 2D simulations were important to gather information, calibrate the model and approach serenely the 3D cases.

Dimension	Discharge m^3/s	Presence of aerator
2D	1500	No
	1900	No
	1500	Yes
	1900	Yes
3D	1500	Yes
	1900	Yes

TABLE 1.1: *Table of cases studied*

1.3 Methodology

Prior to the numerical simulations of the flow, a literature review regarding the background theory of cavitation damages, design of aerators as well as physical and numerical turbulence modeling will be performed. The geometry will be build based on the original layout provided by Vattenfall and the previous work of Penghua Teng on the spillway. An appropiate meshing will be insert to match the geometry and the simulation will be initialized with experimental data. Accuracy, verification and validation of the simulations will be carried out using the flow data received from Vattenfall R&D and empirical results.

1.4 Software

The geometry and meshing process were realized on GAMBIT. It is the program used to generate the geometry and the grid (or mesh) for the CFD solver. While this software is not in the production line anymore (replaced by ANSYS meshing) the learning process is very spontaneous and the meshing capacity are more than enough for a student

project. On the other hand FLUENT, who needs no introduction, was the CFD solver used for the calculations and the post-processing. It contains the physical modeling capabilities needed to model flow, turbulence, heat transfer, and reactions for a wide range of industrial process. The combination of a high Reynolds number and the necessity to accurately locate the interface between multiphase flows on such domain yield to a computationally expensive task.

1.5 Limitations

The calculations were mostly done on a single portable computer and a desk computer which is very limited for such complicated CFD-project. Because of the limited computational power but also the restrained time for the project the reservoir was remove from the simulation. Although the stilling basin was included in the project the lack of computational power did not permit to refine the grid as it should have been to locate the water surface in three dimensions.

1.6 Experimental data

Data from Vattenfall laboratory experiments conduct in 2010 are available but mainly concern the discharge capacity of the spillway, shape of the stilling basin and erosion issues. Attempts were made in the model to study the behavior of air flow but the phenomenon could not be reproduced due to scale effects occurring in such two-phase flow problems. Recently, measure were conducted on the prototype during flood release to estimate the flow and pressure response of the aerator but unfortunately failed. Hence, the assessment of the modeling results will probably be mainly qualitative, but quantitative comparison with available data will be made as much as possible.

Chapter 2

Literature review

2.1 Introduction

A key problem of high-velocity chute flow (damage becomes significant when water velocity exceed 30 m/s corresponding to a head of about 45 meters) is the potential of cavitation damage along the chute bottom and the side walls. Air-added to high speed water flows is known to reduce the risk of cavitation damage, such that chute or spillways are usually secured by sufficient air close to the spillway floor with the aid of aerators.

2.2 Cavitation on spillways

Cavitation is the process of passing from the liquid to the vapor state by changing the local pressure while holding the temperature constant. The local pressure reductions associated with cavitation can be caused by turbulence or vortices in flowing water. (Falvey, 1990). The most common manifestation of cavitation is in hydraulic machinery and hydraulic structures. When the pressure rise again above the vapor pressure, vapor bubble become unstable and collapse, thereby provoking intense pressure and temperature peaks of extremely brief duration. Cavitation in itself is not alarming unless it appears near the boundaries of flow, if the implosions occurs near a solid boundary, e.g. the concrete surface of a chute, the pressures and temperatures generated by the implosion can engender fatigue failure and removal of slight amount of the surface material. These phenomena must be suppressed by all means as it continuously and significantly damage a structure.

It is very challenging and ambitious to anticipate possible cavitation occurrences as the real bubble dynamic process is not yet fully known even if numerous literature is available. Most of the work were based on practical measurement including the flow velocity only. A more assertive approach for the prediction of the risk of cavitation is linked to the cavitation number (or index) σ. This number is derived from Bernoullis equation and defined by

$$\sigma = \frac{p_0 - p_\mathrm{v}}{\rho \frac{U^2}{2}} \tag{2.1}$$

p_0: Local pressure p_v: Vapor pressure of water

ρ: Density of water U: Average flow velocity

All spillways are composed of minor construction flaws such as irregularities at concrete joints or changes due to local settlements. Such irregularities are the starting point of separation of flow, combined with a local pressure reduction behind the irregularities. Based on prototype cavitation damage observation, Falvey (1983) presented a general procedure for spillways depending on the cavitation number.

Cavitation number σ	**Design requirement**
>1.80	No cavitation protection is required
0.25-1.80	The flow surface can be protected by flow surface treatment (e.g smoothing surface roughness)
0.17-0.25	Modification of the design (e.g increasing boundary curvature)
0.12-0.17	Protection by addition of aeration grooves or steps
<0.12	Surface cannot be protected and a different configuration is required

TABLE 2.1: *Criteria for preventing cavitation damage (Falvey,*1983*)*

An important point mentioned by Falvey (1990) declared that the maximum discharge does not automatically cause the minimum cavitation index. Therefore, the cavitation index has to be estimated for all relevant conditions. This can be elucidate in the following manner:

- For limited flow rates, friction prevails. Although flow depths are small, velocities are also modest. Therefore, the cavitation index of the flow can be large enough.

- As the flow rate augments, the proportionate effect of the boundary friction decreases and the flow velocity increases. This cause the cavitation index of the flow to decrease.
- Finally, at much higher flow rates, the increase in flow velocity is negligible. Consequently flow depths are rising and the cavitation index of the flow increases.

To accompany his procedure he also provided an inventory of damage experience in spillways (Fig 2.1) depending on the cavitation number and hours of operation. It should be noted that major damage can happened in less that one month of activity.

2.3 Method to reduce cavitation damage

The prejudicial effects of cavitation erosion may be diminished or canceled by

- Increasing the critical cavitation number (removal of surface irregularities)
- Developing material surface resisting cavitation damages (use of steel fiber concrete, epoxy resins or coating)
- Using a combination of the first two methods (e.g steel lining)
- Directing the cavitation bubble collapses away from the solid boundaries by arranging the structural shape of the structure. However an adequate design is rather difficult to achieve, this option is of a more academic nature and not a feasible

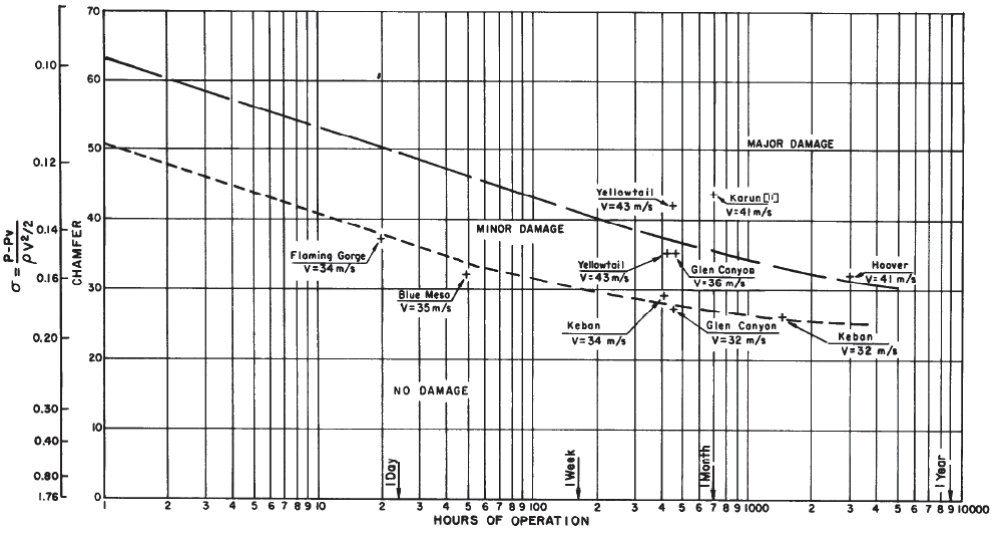

FIGURE 2.1: Damage experience in spillways (Falvey, 1982)

solution for spillways as it is easy understandable an existent spillway is not easily redesigned

- Inducing flow aeration
- The ultimate option, sometimes inevitable from an economic perspective is to allow small deterioration in areas not crucial for the cohesion of the spillway

With velocities greater than 20 to 30m/s, the resilience of surface finish recommended to avoid cavitation are too severe and the cost of cavitation resistant material is exorbitant. For these reasons, it is frequent to preserve the spillway surface from cavitation erosion by introducing air next to the spillway surface using aeration devices placed on the spillway bottom and also on the side-walls.

2.3.1 Effect of air content

In observing flow on an overflow spillway, one normally notes a region of clear water where the water enters the spillway. Then downstream, the water swiftly takes on a milky appearance. It has been established by many researches that the white water and air entrainment begin when the turbulent boundary layer from the floor intersect the water surface. The cases, where the boundary layer create the air entrainment are known as *self aerated flows*.

Free air bubbles in the flow have a favorable effect on cavitation. They prevent the development of sub atmospheric pressure and by increasing the compressibility of the water, greatly reduce the force of the shock from implosion of the bubbles.

The vertical structure of the flow in open channels with highly turbulent flows can be divided into four zones. These are:

- A mixing zone where the water surface is stable
- An underlying zone where air bubbles are dispersed within the water body
- An air free zone

The *upper zone* contained water particles that have been expelled from the mixing zone. It is possible to find water particles at considerable distance above the water surface.

The *mixing zone* consists of a region of surface waves having irregular amplitudes and frequencies. The study of the mixing zone is crucial since all air entrained into the major body of the water or discharged from the flow must traverse this zone.

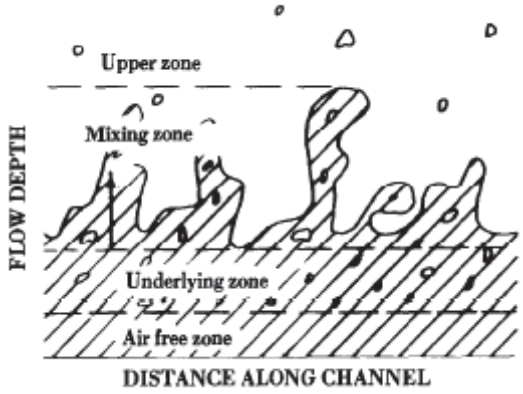

FIGURE 2.2: Structure of aerated open chanel flow (Killen and Anderson, 1969)

The *underlying zone* is an area into which the waves do not enter. The air concentration in this region is determined by the number and size of air bubbles. The main factor affecting the air concentration circulation is the turbulence intensity distribution throughout the flow.

An *air free zone* occurs only in the part of the channel where aeration is still developing. The boundary between the air free zone and the underlying zone cannot be determined exactly.

Numerous experiments and literature have determined that an emulsion with some 5-8% mean air concentration eliminates attack by cavitation, even at very high flow velocities. Note that this is an average air concentration and local air concentration was not recorded precisely before the work of Kramer in 2004, but even if the precise amount of air needed to avoid cavitation damage is not yet fully known, all authors agree that it is wise to promote aeration.

2.4 Air entrainment on spillways

Air may be entrained in water flow in diverse approach but this paper will be focused on free surface aeration and local air supply in chutes.

2.4.1 Self-aerated flow

Self aeration is assured when the chute is long enough to allow a complete development of the boundary layer; it has been adopted to reduce cavitation risk by developing wide

chutes so that, at natural flow rates the flow is close to 1 meter thick once velocities outpace 25-30m/s. As demonstrate before, in a fully turbulent channel, the air content varies substantially; there is a considerable amount at the surface but may be negligible at the bottom. If there are no obstacles or aeration devices, the content will increase progressively from upstream to downstream if the flow is accelerated because of the increased turbulence. Natural aeration of flows where the cavitation risk is apparent is hardly acceptable for adequate protection. By the time it begins to be efficient, the flow has already attained a dangerously high velocity and there is still less than the minimum average air concentration of air at the bottom.

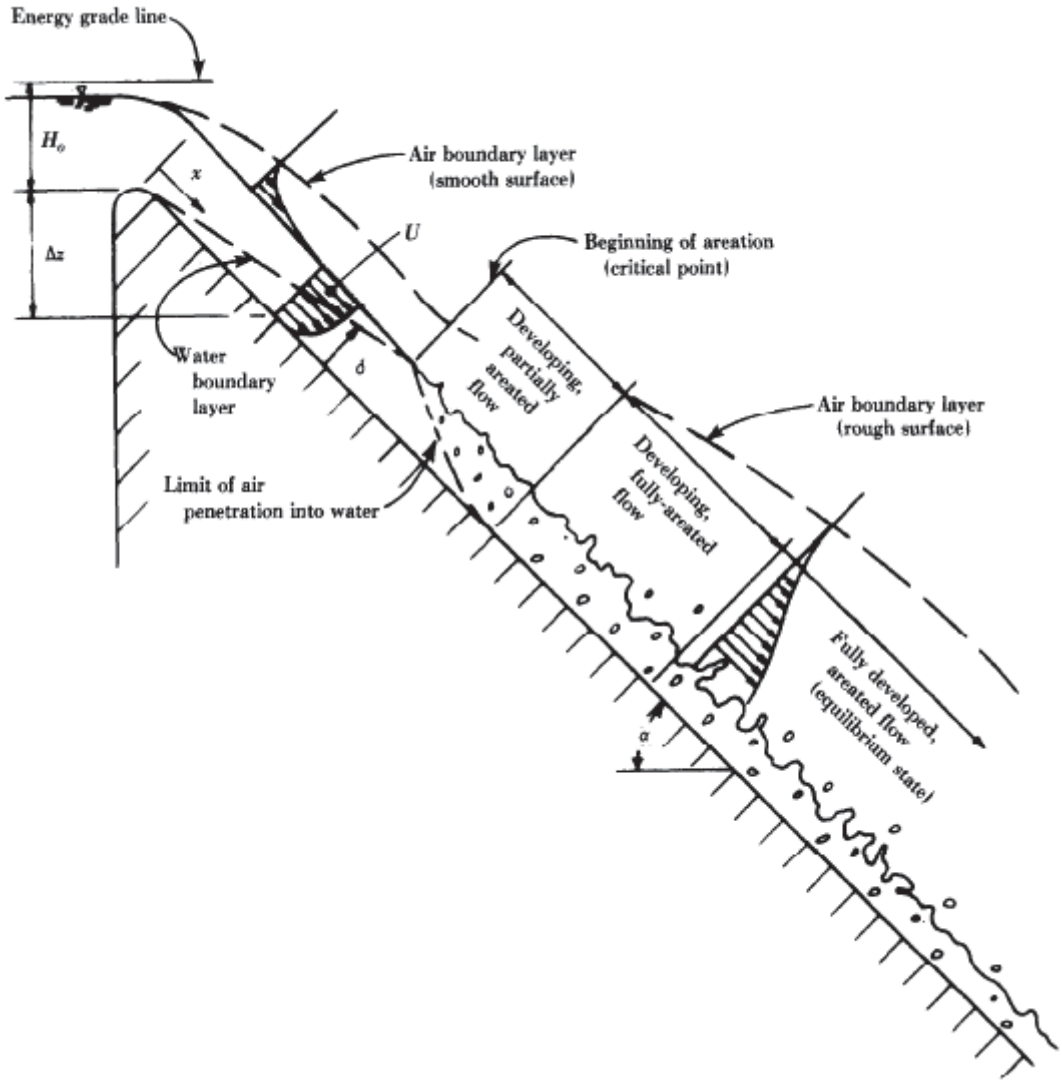

FIGURE 2.3: Air entraining flow regimes in open channel flow (Falvey,1980)

In the longitudinal structure Borman classifies three distinct areas in self-aerating flows.

1. A regime of no air entrainment where the turbulent boundary layer has not attained the water surface
2. A regime of progressing air entrainment in which the air concentration profiles are not constant with distance
3. A regime of established developed air entrainment in which the air concentration profiles are constant with distance.

2.4.2 Artificial aeration

Artificial aeration to prevent cavitation in free-surface flows and on spillway chutes has been largely adopted. The most common method is to design an empty space beneath or at the side of the flow, into which atmospheric air is drawn. In practical terms, this is a step or slot with vent pipes through the wall; for example, the chute floor might be given a wide, deep slot and/or step, and the side wall might have slots, steps, shafts or pipes.

Apparently the first successful utilization of aerators in a hydraulic structure-to avoid cavitation was at Grand Coulee Dam (build between 1933-42). Previous attempts to preserve the surface had failed and after introducing the aerators, reports of damage have stopped. The first known inauguration of aerators in a spillway was at the Bureaus Yellowtail Dam in 1967.

2.4.2.1 Types of aerators

Aerators consist of deflectors, grooves, offsets, and combinations of these. The objective of the deflector is to lift the flow from the boundary so that air can be entrained beneath the flow surface. Thus, air infiltrates the flow without using mechanical systems like air pump-which consume energy. Aeration grooves, slots, or air ducts are used to dispense air across the entire width of the aerator. Lastly, an offset is designed on mild slope to avoid the aerator from being submerged by a fraction of the flow from the jet as it collides with the downstream boundary.

The layout of an aerator reposes on:

- Locating the aerator
- Adjust the ramp or deflector
- Proportioning the air supply duct and air groove

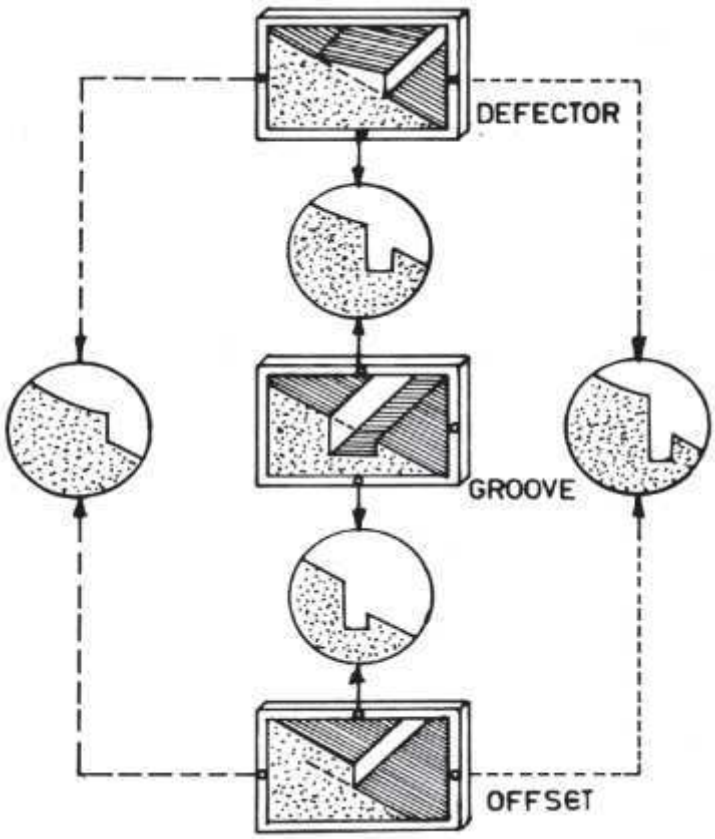

FIGURE 2.4: Types of aerators (Falvey, 1990)

- Dimensioning the offset

The objectives of the aerator design are to build up a device that will preserve the flow surface and not collapse if the aerator happens to be filled with water

Location of aerators Placement of an aerator on a chute to keep the cavitation index higher than 0.20 is a criterion difficult to achieve in actual practice. That is why free surface aeration is often neglected and simple approach are often used to determine the location of aerators, over sizing the number of aerator is also a solution to stay on the safe-side . It should also be emphasized that aerators are not always placed according to aeration guideline but are also subject to other feature of the flow or to the structure's design.

Ramp design The function of the ramp is to lift the flow away from the lower boundary of the chute. Thereby, the free trajectory patterns allow the underside of the nappe to become aerated. When flow once again joins the boundary, it has entrained enough air to prevent cavitation damage on the downstream flow surface.

Air vent design Numerous methods have been designed to vent air from the atmosphere to the underside of the nappe. These include the following:

- Ramps or deflectors on sidewalls
- Offset sidewalls
- Piers in the flow
- Slots and duct in sidewall
- Duct system underneath the ramp
- Duct system downstream of ramp

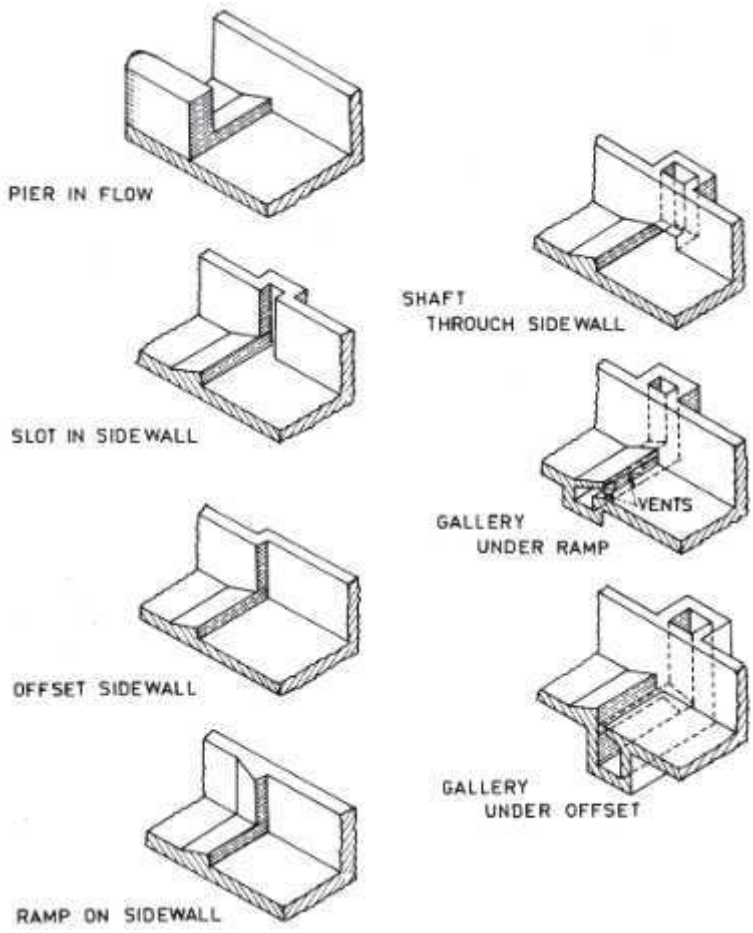

FIGURE 2.5: Air supply to aerators (Falvey, 1990)

Ramps, offset sidewalls, and piers in the flow and slots in walls are generally used to furnish aeration downstream of control gates. However, these air vent types are not common on wide chutes because the required offsets are unreal from a structural point of view. A duct beneath the ramp is used on wide chutes, the system of ducts and vents

ensures suitable aeration of the flow and are used when the required slot size or sidewall offsets are disproportionate.

Estimation of Air entrainment Capacity Several empirical expressions have been suggested for the air entraining capacity below the nappe but these equations not always results in good prediction of air flow rates. Nevertheless, it has been decided to present some of these equation to compare with the computational result as the experimental data concerning air entrainment are not available. Two approaches are presented for the air entrainment coefficient, first an indirect approach based on the length of jet after aerator and a direct approach based on the analysis of the geometry.

The indirect approach presented by Glazov (1984) and take over by Favley (1990) appears to be one of the most accurate. The unite discharge of air is given by :

$$q_a = U_i \Big\{ [(X_i - X_n)^2 + (Y_i - Y_n)^2]^{1/2} - \frac{q_w}{2U_i} \Big\} \tag{2.2}$$

X_i: Horizontal distance from end of ramp to jet impact location
X_n: Horizontal distance from end of ramp to centerline of jet at impact location
Y_i: Elevation at impact point
Y_n: Elevation of centerline of jet at impact point
q_w: Unit discharge of water
U_i: Average flow velocity

An other reliable equation is computed by Rutschmann and Hager (1990) based on numerous experimental data (1988), tested on Chanson's data (1988) and validated by Gaskin (2003).

$$\beta_{max} = \frac{q_a}{q_w} = (\tan\alpha)^{1.15} \exp[(1.15 \tan\theta)^2](Fr - 5.4)^{0.35} \tag{2.3}$$

q_a: Unit discharge of air
q_w: Unit discharge of water
α: Ramp angle
θ: Spillway slope

Concerning mean air concentration, asssuming a gradually varied flow region with a constant rate of air entrainment, Chanson (1988) assumes that :

$$C_a = \frac{\beta}{1 + \beta} \tag{2.4}$$

As said before the vertical distribution of air is not uniform. It is obvious that air in the surface and middle layers does not protect the surface from cavitation damage but influence greatly the mean concentration hence it is not possible to judge the degree of protection of the surface only with the mean concentration. In conclusion, the question of air concentration distribution is not approached since the behavior of the air downstream of an air device supply and free-surface aeration are not subjects of this research.

2.4.2.2 Aerator submergence

Experienced observer have noticed that equation (2.3) is practical only for Froude number above 5.4. It does not mean air entrainment is impossible for a Froude number below this value but only that the air entrainment capacity is no more linear with the geometry of the structure. However Chanson (1995) proved that for a low Froude number the filling of ventilated cavities behind spillway aerators may occur. As a result, aerator submergence could happen for discharges lower than the design discharges. The submergence of aerators must be avoid as the aeration device would stop preventing cavitation damage and might even act as a cavitation generator, even at low Froude number.

The condition for cavity filling are according to Chanson (1988) and Shi (1983)

$$Fr_o < 2.77 + 0.94\frac{d_0}{t_s} \tag{2.5}$$

$$Fr_o < 2.86\cos\theta\cos\alpha\sqrt[3]{\frac{d_0}{t_r}} \tag{2.6}$$

d_0: Depth of flow at the beginning of the ramp
t_r: Ramp height
t_s: Offset/duct height

Note that this relations have been validated for aerator with ramp and offset.

Chapter 3

Theory

3.1 Governing equations for CFD

The instantaneous continuity equation (3.1), momentum equation (3.2) and energy equation (3.3) for a compressible fluid can be express as:

$$\frac{\partial \rho}{\partial t} + \frac{\partial}{\partial x_i}(\rho u_i) = 0 \tag{3.1}$$

$$\frac{\partial}{\partial t}(\rho u_i) + \frac{\partial}{\partial x_j}(\rho u_i u_j + p\delta_{ij} - \tau_{ji}) = 0 \tag{3.2}$$

$$\frac{\partial}{\partial t}(\rho e_0) + \frac{\partial}{\partial x_j}[\rho u_j e_0 + u_j p + q_j - u_i \tau_{ij}] = 0 \tag{3.3}$$

For a Newtonian fluid, assuming Stokes Law , the viscous stress is defined by:

$$\tau_{ij} = 2\mu S^*_{ij} \tag{3.4}$$

Where the trace-less viscous strain-rate is given by:

$$S^*_{ij} \equiv \frac{1}{2}\left(\frac{\partial u_i}{\partial x_j} + \frac{\partial u_j}{\partial x_i}\right) - \frac{1}{3}\frac{\partial u_k}{\partial x_k}\delta_{ij} \tag{3.5}$$

These equations are often referred to as Navier-Stokes equations. The solution of the Navier-Stokes equations is a flow velocity field since it is defined at every point in a domain and an interval of time. Once the external body forces are added (i.e gravity) and the velocity field is computed, other quantities of interest, such as pressure or

temperature, may be found. The energy equation will not be used in the following project since the thermal aspect of the fluid is not decisive to answer the problematic.

3.2 Turbulence Model

Most flows of engineering significance are turbulent. Turbulence is associated with the existence of random fluctuations in the fluid. Although the conservation equation remain applicable, the dependent variable, such as the transient velocity must be interpreted as an instantaneous velocity which is impossible to predict as the fluctuating velocity occurs randomly with time. Instead, the velocity can be decomposed into a steady mean value $\bar{u_i}$ with a fluctuating component u_i'.

$$u_i = \bar{u_i} + u_i' \tag{3.6}$$

This process of time averaging is called Reynolds decomposition. This decomposition integrate in the instantaneous continuity and momentum equation yield to the Reynolds-averaged Navier-Stokes (RANS) equations .

$$\frac{\partial}{\partial t}\left(\rho u_i\right) + \frac{\partial}{\partial x_j}\left(\rho u_i u_j\right) = -\frac{\partial p}{\partial x_i} + \frac{\partial}{\partial x_j}\left[\mu\left(\frac{\partial u_i}{\partial x_j} + \frac{\partial u_j}{\partial x_i} - \frac{2}{3}\delta_{ij}\frac{\partial u_k}{\partial x_k}\right)\right] + \frac{\partial}{\partial x_j}\left(-\rho\overline{u_i' u_j'}\right) \tag{3.7}$$

Here the overbar on the mean velocity has been dropped for the sake of readability and the continuity equation overlooked as the averaged and instantaneous equation share the same expression with this notation. The RANS equations contain more unknowns than equations, these unknowns are the Reynolds Stress terms, and must be modeled to close these set of equations.
This paper will only presents the two-equation turbulence models but the reader should be aware that many closure models exist. The Boussinesq hypothesis (1877) postulated that the effect of turbulence can be represented as an increased viscosity, it is the eddy viscosity model.

$$-\rho\overline{u_i' u_j'} = \mu_t\left(\frac{\partial u_i}{\partial x_j} + \frac{\partial u_j}{\partial x_i} - \frac{2}{3}\frac{\partial u_k}{\partial x_k}\delta_{ij}\right) - \frac{2}{3}\rho k\delta_{ij} \tag{3.8}$$

The simplest “complete models” of turbulence are two-equation models in which the

solution of two separate transport equations allows the turbulent velocity and length scales to be independently determined. The realizable k - ϵ model is part of this class of turbulence model. The robustness, the accuracy and the computational price of its "father",the k - ϵ model, explain its popularity in CFD. The k - ϵ model is a semi-empirical model where the equations relies on phenomenological considerations and empiricism. Improvements have been made to correct its weakness and variants like *RNG* k - ϵ model and the realizable k - ϵ model are now promoted by FLUENT. The realizable k - ϵ model is an evolution and contrasts with the standard k - ϵ model in two essential ways:

- The realizable k - ϵ model involves a new formulation for the turbulent viscosity
- A new transport equation for the dissipation rate ϵ

The term "realizable" implies that the model satisfies certain mathematical constraints on the Reynolds stresses, consistent with the physics of turbulent flows. Neither the standard k - ϵ model nor the *RNG* k - ϵ model is realizable. The realizable k - ϵ model grant preferable performance for flows involving rotation, boundary layers under strong adverse pressure gradients, separation, and recirculation.

The modeled transport equations for k and ϵ in the realizable k - ϵ model are

- for turbulent kinetic energy k

$$\frac{\partial}{\partial t}(\rho k) + \frac{\partial}{\partial x_i}(\rho k u_i) = \frac{\partial}{\partial x_j}\left[\left(\mu + \frac{\mu_t}{\sigma_k}\right)\frac{\partial k}{\partial x_j}\right] + P_k + P_b - \rho\epsilon - Y_M + S_k \quad (3.9)$$

- for dissipation ϵ

$$\frac{\partial}{\partial t}(\rho\epsilon) + \frac{\partial}{\partial x_j}(\rho\epsilon u_j) = \frac{\partial}{\partial x_j}\left[\left(\mu + \frac{\mu_t}{\sigma_\epsilon}\right)\frac{\partial \epsilon}{\partial x_j}\right] + \rho C_1 S\epsilon - \rho C_2 \frac{\epsilon^2}{k + \sqrt{\nu\epsilon}} + C_{1\epsilon}\frac{\epsilon}{k}C_{3\epsilon}P_b + S_\epsilon \quad (3.10)$$

where

$$C_1 = \max\left[0.43, \frac{\eta}{\eta + 5}\right], \qquad \eta = S\frac{k}{\epsilon}, \qquad S = \sqrt{2S_{ij}S_{ij}}$$

As in other k - ϵ models, the eddy viscosity is computed from

$$\mu_t = \rho C_\mu \frac{k^2}{\epsilon} \quad (3.11)$$

Here however C_μ is no longer a constant like in the basic k - ϵ model but computed with empirical constants and variables depending on the rate of rotation and strain rate. The

production of turbulent kinetic energy is derived from

$$P_k = -\rho\overline{u_i' u_j'}\frac{\partial u_j}{\partial x_i} \tag{3.12}$$

in a manner consistent with the Boussinesq hypothesis, we have

$$P_k = \mu_t S^2$$

The effect of Buoyancy

$$P_b = \beta_{Buoyancy} g_i \frac{\mu_t}{\mathrm{Pr}_t}\frac{\partial T}{\partial x_i} \tag{3.13}$$

Finally the effect of compressibility

$$Y_M = 2\rho\epsilon \mathrm{M}_t^2 \tag{3.14}$$

with M_t defined as the turbulent mach number $\mathrm{M}_t = \sqrt{\frac{k}{a^2}}$

3.3 VOF Model

The VOF formulation is based on the fact that two or more fluids are immiscible. Each phase is defined by a variable which expresses the volume fraction of the phase in the cell. In each control volume, the sum of the volume fraction of all phases is equal to one. Variables and properties in any cell are either representative of one of the phases, or representative of a mixture of the phases, depending of the volume fraction values. In other words, if α_q stand for the volume fraction of the q^{th} fluid in a cell then the three possibilities for a given cell are:

- $\alpha_q = 0$: The cell is empty of the q^{th} fluid
- $\alpha_q = 1$: The cell is full of the q^{th} fluid
- $0 < \alpha_q < 1$: The cell contains the interface between the q^{th} fluid and one or more other fluids

In order to determine the location of the interface between the phases a continuity equation for the volume fraction of one of the phases is solved. For the q^{th} phase, this

equation has the following form:

$$\frac{1}{\rho_{\mathrm{q}}}\left[\frac{\partial}{\partial t}(\alpha_q\rho_q)+\nabla\cdot(\alpha_q\rho_q\vec{u}_q)=S_{\alpha_q}+\sum_{p=1}^{n}(\dot{m}_{\mathrm{pq}}-\dot{m}_{\mathrm{qp}})\right] \tag{3.15}$$

This equation will be solved through explicit time discretization by the numerical solver.

$$\frac{\alpha_q^{n+1}\rho_q^{n+1}-\alpha_q^n\rho_q^n}{\Delta t}V+\sum_i(\rho_q V_f^n\alpha_{q,i}^n)=\left[\sum_{p=1}^{n}(\dot{m}_{\mathrm{pq}}-\dot{m}_{\mathrm{qp}})+S_{\alpha_{\mathrm{q}}}\right]V \tag{3.16}$$

Finally the momentum equation is resolved throughout the computational domain, and the phases share the resulting velocity field. The momentum equation is dependent on the volume fractions of all phases through the properties ρ and μ.

For free surface flow where the shape of the interface is of interest and with relatively homogeneous velocity, the volume fractions are close to zero or unity except near the interface and the VOF method is particularly recommended.

Chapter 4

Bergeforsen dam

4.1 Site description and adaptations

Bergeforsen is a town with around 1600 inhabitants located in northern Sweden. The town is crossed by the river Indalsälven which has an average flow of $444m^3/s$ and an average high flow of $1110m^3/s$ (SMHI,2009)

There are 31 power plants in operation in Indalsälven and the facility at Bergeforsen was operational in 1955. The power plant is a run-of-the river type meaning the dam has limited storage capacity. The plant utilizes four Kaplan turbines for a total turbine flow of $840m^3/s$ and an installed electrical capacity of $168MW$. The former spillway (still in activity) consists of three 15 meters wide openings with upward going radial gates and has a sill elevation of +113,75 meters (the elevation are defined as the meters above sea level plus 100 meters in order to avoid negative heights). This spillway can discharge around $2300m^3/s$ at the full reservoir retention level (FRRL), $123{,}0m$

In accordance with the new Swedish design flood guidelines the design flood for the Bergeforsen dam has been revised from $2300m^3/s$ to $3500m^3/s$. To be able to upgrade the former spillway and increase the safety requirement of the structure and in the same time respond to the demand of the flood guidelines it has been suggested to construct a separate second spillway.

The new spillway consists of an inlet, a stilling basin with aerator, a curved tunnel and an outlet. It is equipped with a 25 meters wide gate, the largest in Sweden. The spillway can discharges around $1500m^3/s$ at the normal reservoir retention level. The sill elevation is fixed to +112, 75 meters, the stilling basin is 85 meters long and 35

meters wide and is 25 meters below the spillway threshold elevation. However the new spillway is located relatively far to the north, therefore the tunnel gets an unfavorable sharp bend to lead the water to the river channel. This can lead to unwanted turbulent flow and wave motions which affect the flow pattern negatively and reduce the safety margin. By rounding the transition from the stilling basin to the tunnel these effects are decreased.

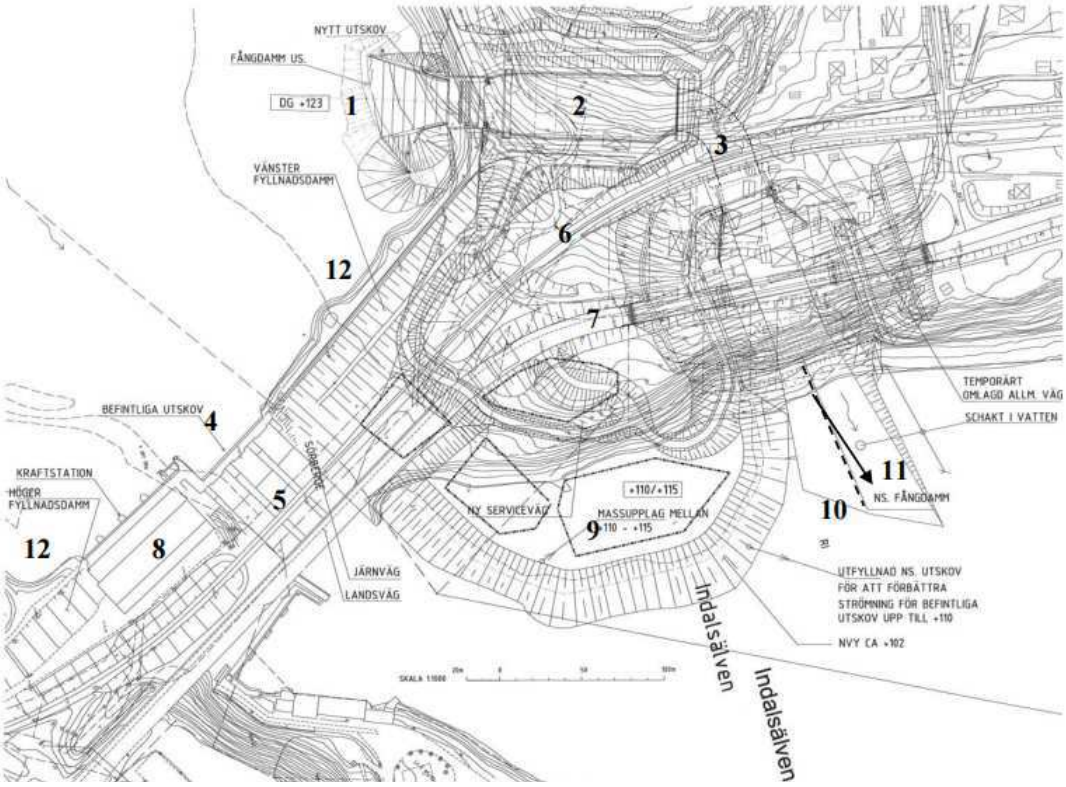

FIGURE 4.1: Layout of the new spillway (Ekstrom, 2011)

1. New spillway inlet
2. New spillway stilling basin
3. Tunnel section
4. Previous spillway inlet
5. Previous spillways chutes
6. Railroad
7. Higway
8. Power plant
9. Excavated material
10. Outlet centerline axis
11. Main direction of flow
12. Earth fill dam

FIGURE 4.2: Spillway inlet viewed from downstream with aerator submerged

Chapter 5

Numerical model and setup

5.1 Solver

The default algorithm, the pressure-based segregated solver, is used in Fluent with the PISO pressure-velocity coupling scheme. This algorithm is highly recommended for transient flow calculations. When using a large time step or on meshes with a high degree of distortion PISO can maintain a relatively stable calculation. The Fluent user guide strongly recommend the PRESTO! scheme coupled with the Geo-Reconstruct method for the volume fraction. This combination can be computationally expensive but grant a sharp interface between phases. An explicit scheme is used with the VOF method and the Courant number is initialized at 2 to use a variable time stepping method. Notable is the fact that it was not necessary to change the under-relaxation factor in order to obtained suitable residuals.

5.2 Computational domain and grid

The flow over the spillway is modeled both in two and three dimensions, in the 3D case we can use the symmetry of the chute, the aerators and stilling basin to divide our numerical domain in half. The reservoir was voluntary put aside from the project to minimize the computational cost, only a small part before the threshold, the chute with the aerators/shaft and the stilling basin before the tunnel were modeled. The creation of the geometry was based on authentic layout of the spillway and realized, in parallel with the meshing, on the software GAMBIT. Six different transient flows cases were studied with discharges of approximately 1500 and 1900m3/s in two and three dimensions on FLUENT.

5.2.1 2D-cases

The two dimensions cases domain is based on the cross section of the three dimensions domain (more specifically on the symmetry cross section). The domain is approximately 180 meters long and 40 meters high. After discussion with the supervisor the exact position of the outlet was not respected and the stilling basin extend in order to avoid divergence caused by the hydraulic jump too close from the strict boundary condition at the outlet.

5.2.1.1 2D-case without aerator

Prior to the numerical simulation of air entrainment, a two dimensions case without aerator was designed in order to comprehend the flow behavior without aeration. The maximum velocity, the pressure distribution and the shape of the hydraulic jump were the main property to display to judge the risk of cavitation damage.

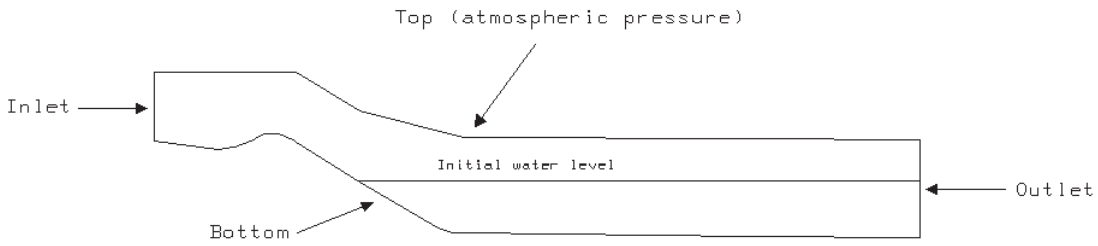

FIGURE 5.1: 2D-domain without aerator

Grid The grid is build of quadrilaterals cells on the whole domain. Expecting high velocity at the bottom of the chute, the mesh was build up to be detailed enough to have an appropriate Courant number. It resulted in a mesh of 240,000 cells and a time consuming modeling. Considering the limited computational power and period to hand the project this number of cell was reduced on the following 2D-simulations.

Boundary condition A pressure inlet boundary was applied with the open channel option, the flow specification method used was to determined the free surface level and velocity to match the required flow (note that in this case water and air share the same velocity at the inlet). At the outlet a pressure condition was also defined with a specified free surface level. The top is considered as a pressure inlet with an atmospheric pressure

and a limited turbulent intensity. Concerning the walls, a no-slip condition was used and a roughness of 0.3mm imposed on the wall in addition with the default roughness constant of 0.5.

5.2.1.2 2D-case with aerator

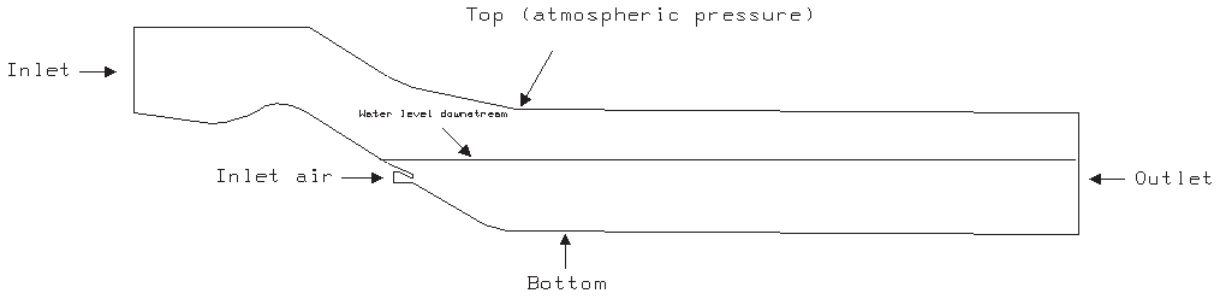

FIGURE 5.2: 2D-domain with aerator

Grid The grid is constitute of quads cells, to resolve the turbulent boundary layer the hex-mesh is thinner close to the bottom of the spillway and in the aerator. It results in a mesh of 150,000 cells

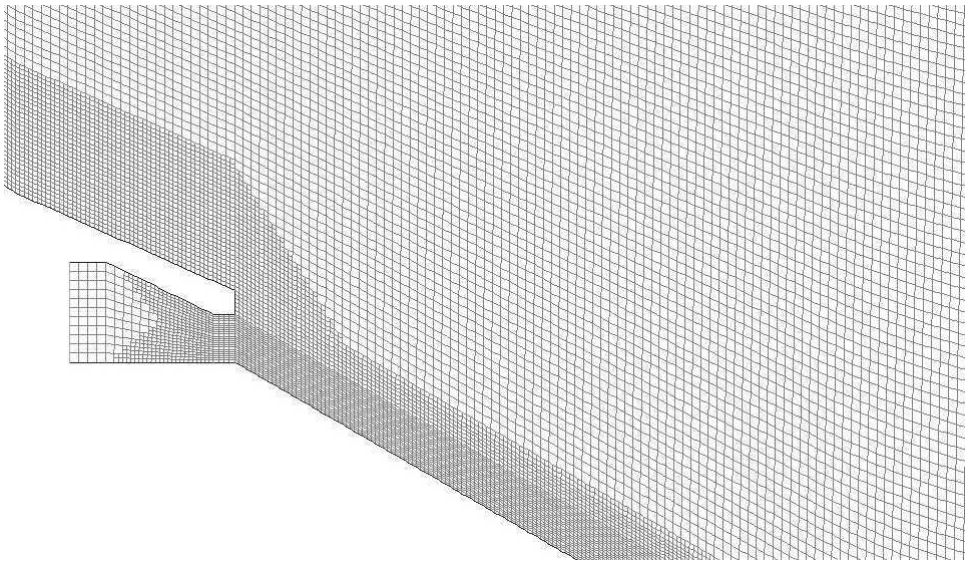

FIGURE 5.3: View of the thinner hex-grid near the bottom and aerator

Boundary condition The boundary condition remain identical to the case without aerator, however the back-wall of the aerator was considered as an inlet with an atmospheric pressure to estimate the air flow driven by the water flow.

5.2.2 3D-cases

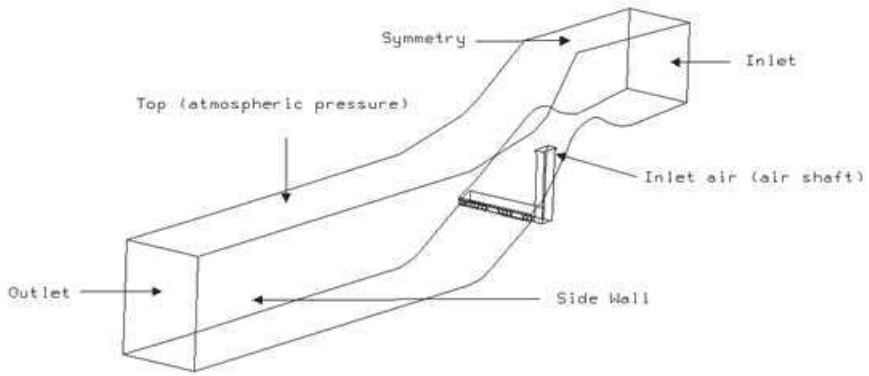

FIGURE 5.4: 3D-domain

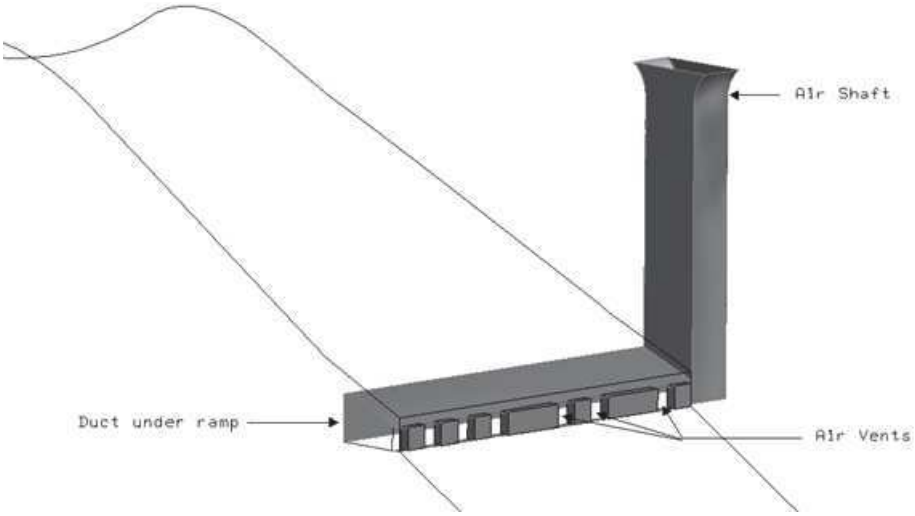

FIGURE 5.5: 3D-domain : View on the air shaft and vents

On the figure 5.5 the aerator part are shaded, it is easy to identify the shaft through the sidewall and the gallery under the bottom ramp. Thirteen air vents are present on the prototype and half of them are presented on the model. The positioning of the air-vents is respected by the symmetry.

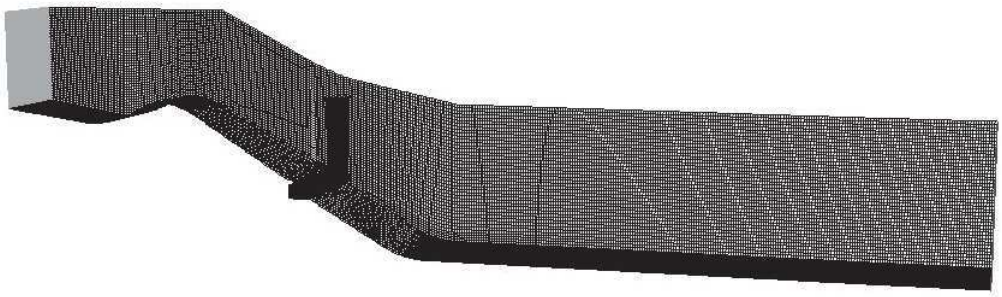

FIGURE 5.6: 3D-domain : View of the grid

Grid The grid is made of hexahedra-cells (also known as hex-mesh) as much as possible but the aerator part is constituted of a thinner unstructured mesh due to the complex geometry. It results in a computationally expensive mesh of 980,000 cells.

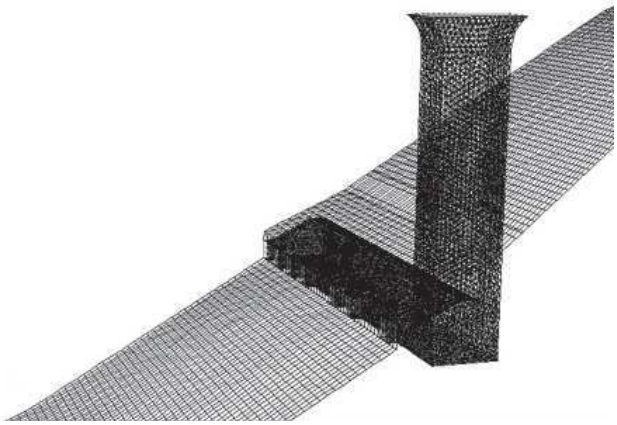

FIGURE 5.7: 3D-domain : View of the unstructured mesh

Boundary condition The boundary condition were similar to the 2D case, the hydraulic diameter were adapted to the new geometry, the inlet for the air flow placed at the top of the air shaft and the symmetrical cross-section defined.

In the table 5.1 the mean size cell helps to visualize the extent of a cell and highlight the probable uncertainties linked to the spatial resolution.

Dimension	Discharge m^3/s	Presence of aerator	Number of cells	Mean size cell (m)
2D	1500	No	240,000	0.12x0.12
	1900	No	240,000	0.12x0.12
	1500	Yes	150,000	0.15x0.15
	1900	Yes	150,000	0.15x0.15
3D	1500	Yes	980,000	0.38x0.38x0.38
	1900	Yes	980,000	0.38x0.38x0.38

TABLE 5.1: *Recap of the grid used in function of the case simulate*

Chapter 6

Results and discussion

This chapter presents the result for diverse properties of the discharge coupled with air entrainment and behavior of the fluid in the stilling basin. The hydraulic aspects that are investigated are principally the volume fraction of water, the velocity and pressure peak of the fluid and finally the air entrainment ratio. An overview of the cases studied is given below. The time steps were variable and determined by the Global Courant number (approximate range of time step: [0.005;0.05] seconds). The variable time steps allows a better flexibility depending on the behavior of the flow.

Dimension	Discharge (m^3/s)	Aerator	Global Courant Number	Number of iterations	Length of simulation (s)
2D	1500	No	3	136,000	35
	1900	No	3	143,000	36 (first 30s $1500m^3/s$)
	1500	Yes	2	475,000	117
	1900	Yes	2	352,000	114
3D	1500	Yes	5	29,400	46.5
	1900	Yes	5	46,500	50 (first 40s $1500m^3/s$)

TABLE 6.1: *Results*

6.1 Results

6.1.1 Necessity of an aerator

In the case of the geometry without aerator, the spillway slope is constant and equal to 32°from the threshold to the stilling basin as it is the angle of the chute before the ramp. As suggested by Falvey in his design procedure for aerators, observations bear on

the cavitation number linked to the velocity and pressure inside the fluid. Experiments were made for the flows cases studied later on.

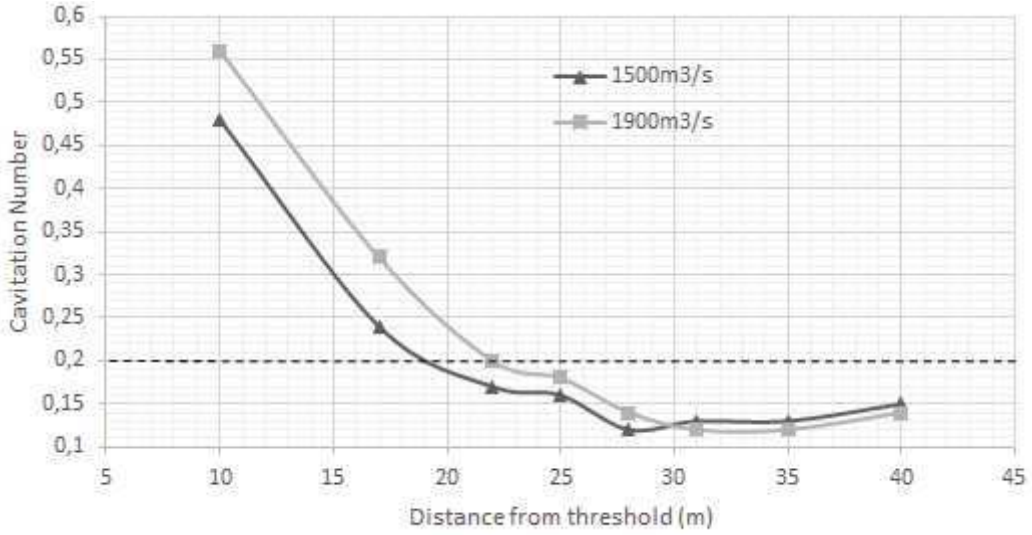

FIGURE 6.1: Cavitation Number in function of the distance from the threshold

On the Fig 6.1 , it is clear that the cavitation number is below the limit fixed by Falvey and the risk for cavitation damage not negligible 20 meters after the threshold. The cavitation number reaches its minimum before hitting the stilling basin where the velocity of the fluid is maximum. On the prototype the ramp start 20 meters after the threshold and the actual aerators 25 meters after which is consistent with the data presented.

However, it should be noted that this result are quite pessimistic and the risk probably overestimate. Since the cavitation damages depends on the flow properties close to the spillway it is recommend to consider the boundary layer growth as the fluid descends and not the mean flow velocity as it has been done here. A solution would have been to introduce a velocity at a distance k from the surface U_k. Yet the limited precision of the grid coupled with the no-slip condition do not permit a proper observation of the boundary layer and the actual velocity inside it. The choice of the mean flow velocity was therefore reasonable and adapted to the present resolution.

6.1.2 Water surface profile

The water level surface is an interesting component of the flow behavior as it will be comparable with data from the VATTENFALL's model and will permit to calibrate and evaluate the validity of the computational modeling but a theoretical problem occurred promptly with the 2D simulations.

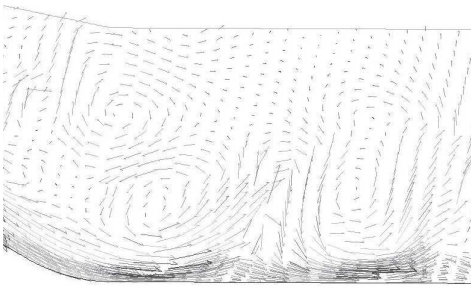

FIGURE 6.2: 2D: Vorticies in bassin

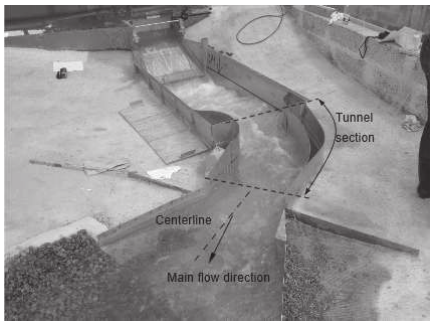

FIGURE 6.3: Physical hydraulic model for the new spillway (Yang)

It is observable on the Fig. 6.2 that large scales vortices of several meters are establish. Once formed this vortices can move, stretch or twist in a complex ways and in three dimensions. The turbulent behavior of the flow in the stilling basin is clearly anisotropic and all the characteristics scales have an importance. Therefore the 2D simulations neglects some physical understanding and modeled poorly turbulence in the stilling basin. (e.g For large scale flows, such as atmospheric or oceanic turbulence, a precise 2D simulation can be performed because the third dimension is negligible compared to the two first which is not the case in the basin)

The 3D simulation with a discharge of $1500 m^3/s$ was the case used to compare with experimental data from VATTENFALL obtained with the hydraulic model on Fig 6.3. The cross section used to determine the water surface was located exactly at the middle of the chute (e.g the symmetry cross section) as it is where the flow is fully developed and not affected by the side walls.

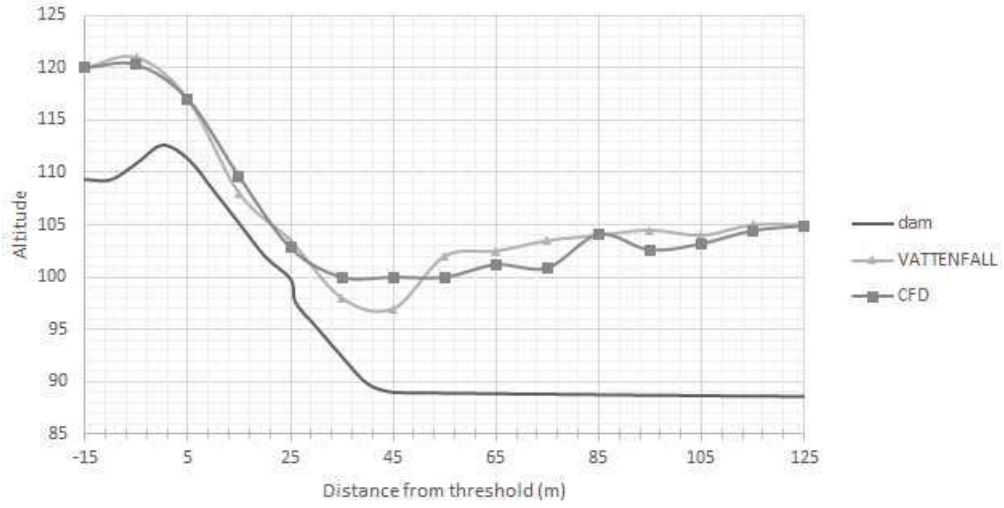

FIGURE 6.4: Comparison of the water surface level in the 3D numerical model and the experimental data

The water surface level is as expected from the boundaries conditions respected in the reservoir and at the end of the basin. Despite the poor precision a resemblance in the flow behavior is noticeable above the chute and in the basin. The main difference is found on the shape of the hydraulic jump which is more pronounced on the experimental data.

6.1.3 Velocity and flow circulation

The velocity on the chute and the flow circulation are essential features of the flow and must be examine to fully understand the behavior of the fluid and determine the level of risk due to cavitation damage.

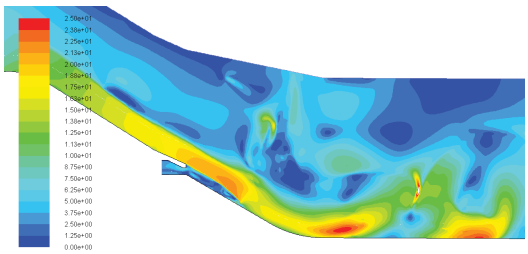

FIGURE 6.5: Velocity magnitude on the chute (2D-1500m^3/s)

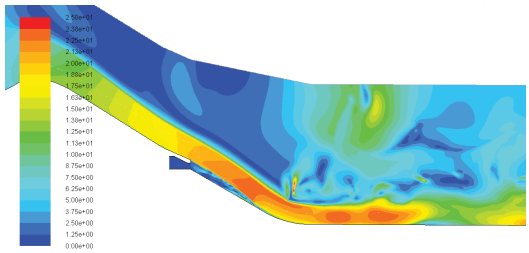

FIGURE 6.6: Velocity magnitude on the chute (2D-1900m^3/s)

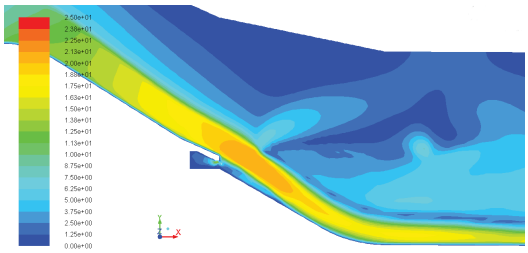

FIGURE 6.7: Velocity magnitude on the chute (3D-1500m^3/s)

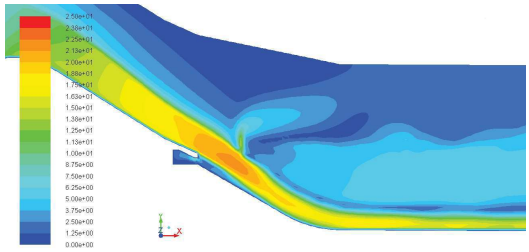

FIGURE 6.8: Velocity magnitude on the chute (3D-1900m^3/s)

As expected the larger the discharge the higher the velocity, on all cases the velocity reaches valor large enough to justify the existent of an aerator

The difference of velocity magnitude between the three and two dimensional case is easily explicable by the water level surface in the stilling basin. In the 3D cases, the water level in the basin is high enough and relatively stable to absorb the water jet and reduce its velocity on a short interval. On the other hand, in the 2D cases the water jet hit the basin much later and reduce its velocity in a greater interval. As said before the 2D cases probably overestimate the velocity and turbulence in the basin. Therefore the study on the fluid circulation has only been performed on the 3D cases.

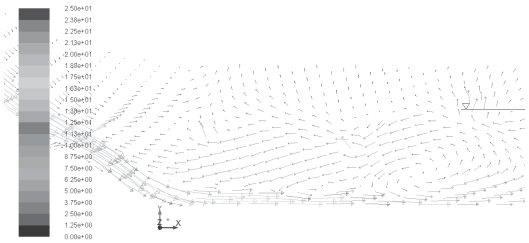

FIGURE 6.9: Fluid circulation (X-direction-1500m^3/s

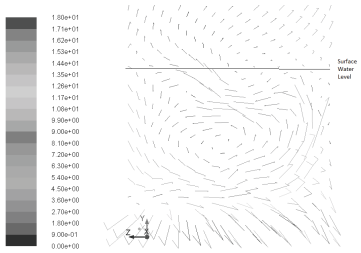

FIGURE 6.10: Fluid circulation (Z-direction with wall at the right-1500m^3/s

On Fig. 6.9 the recirculation of the fluid in the stilling basin is clear. The fluid comes away from the bottom as the velocity decrease and a fraction of that fluid come back near the hydraulic jump with a relatively low velocity keeping the water surface level high. On the Fig. 6.10, the circulation missing on the 2D case is presented. Even if the circulation is slower than the X-direction it is not negligible as it dissipates energy which was conserved in two dimensions.

6.1.4 Pressure at the bottom

In order to investigate the stress on the chute and the trigger of air entrainment some pressure investigation were carry out on the 3D cases and verify by the 2D cases on the bottom of the spillway.

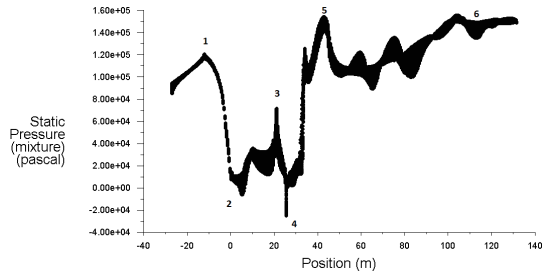

FIGURE 6.11: Static gauge pressure on the bottom of the chute (3D-1500m^3/s)

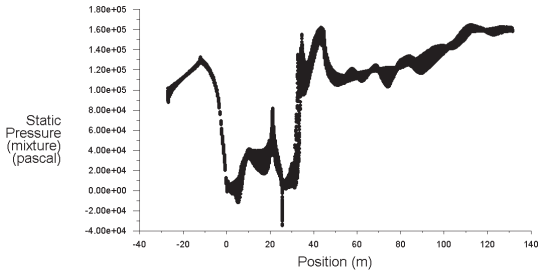

FIGURE 6.12: Static gauge pressure on the bottom of the chute (3D-1900m^3/s)

In the interest of clarity static and dynamic pressure were represented apart. We can clearly identify the distinct region of the chute (items were marked on the Fig. 6.5)

1. A peak of the static pressure before the gate were the water depth is maximum, the low velocity lead to a negligible dynamic pressure

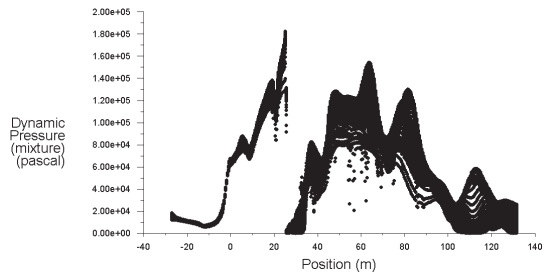

FIGURE 6.13: Dynamic pressure on the bottom of the chute (3D-$1500m^3/s$)

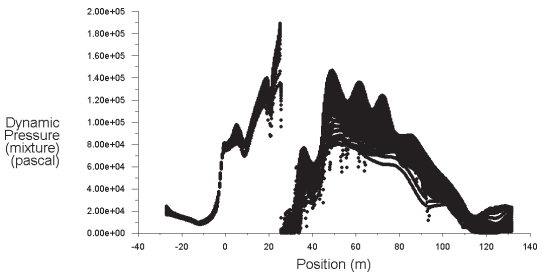

FIGURE 6.14: Dynamic pressure on the bottom of the chute (3D-$1900m^3/s$)

2. At the crest (x=0m) the water depth decrease and the velocity increase which lead to a joint behavior for the static and dynamic pressure

3. The peak in the static pressure is due to the sudden change of slope in the chute (which match the start of the ramp, the velocity of the flow is still increasing with the dynamic pressure

4. A sudden gradient create by the aerator, the relative pressure became negative as expected in the nappe below the flow. The dynamic pressure is no-existent as the fluid does not touch the bottom anymore

5. The fluid hit back the bottom strongly and the large velocity coupled with the abrupt change of angle (between the slope of the chute and the basin) yield to substantial pressure force.

6. The velocity drop on the stilling basin and the water level surface stabilize itself leading to a weak dynamic pressure and a relatively constant static pressure.

Even if the study of the pressure force was not the main subject of this paper, the comprehension of it is primordial to design the structure of the dam and also to understand the phenomenon of air entrainment as it is the difference of pressure between the atmosphere and the nappe below the flow that will drag the air into the shaft.

6.1.5 Air entrainment

The air entrainment was the major and most challenging part of this study and simulations. Despite the poor modeling of the basin the study were first mainly based on the 2D cases. As it is computationally inexpensive compare to the 3D, it was easier to wait for the flow to be fully developed and the record of air entrainment were made during a period of 50 seconds which lead to a computational period of 120 seconds.

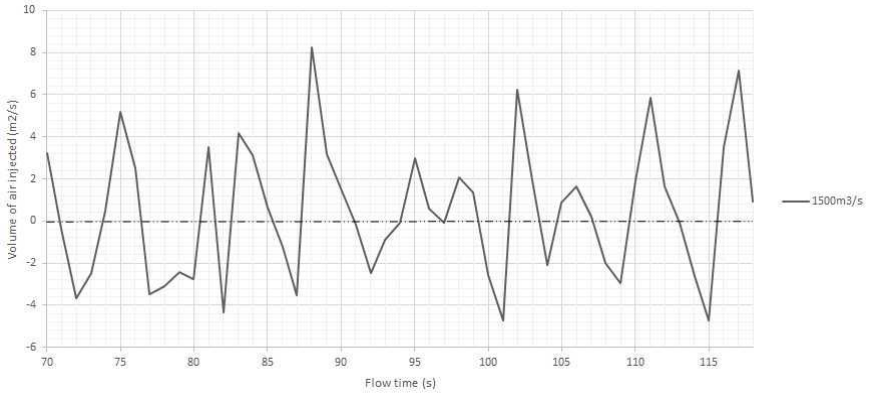

FIGURE 6.15: Air flow injected at the aerator in function of flow time (2D-1500m^3/s)

The results were not satisfying and probably underestimate. The air flow was fluctuating on very short period (the Fig 6. represents an average for clarity) and more disturbing backflow effect was common. It results in an average of 18.2m^3/s (20.5m^3/s for the 1900m^3/s flow) of air injected by the flow after extrapolation. This result are lower than what was expected and are furthermore probably overestimate and uncertain on many points :

- The back wall of the aerator was considered as an inlet with an atmospheric pressure boundary condition. This unavoidable simplification ease the injection of the air by canceling the friction loss as the source is much more closer than it should be in the 3D case.
- The unit discharge was extrapolate by multiplying it by the width of the aerator. This does not respect the original geometry by enlarging the surface of the air inlet.
- The inlet was subject to backflow effect with air but also some water. In the VOF method the fluid is considered as a "mixture" and the proportion of water and air was determined during the post-processing with some uncertainties and simplifications.

However this pre-work was important to approach serenely the 3D cases and gather information. On the 3D cases the inlet was placed at the top of the shaft. This position suit well the model because the mixture consist only of air at this altitude and facilitate the post-processing.

Once again, the result were not reliable. The simulation was shorter due to the cost of such modeled but no improvement is seen after the establishment of the flow. The

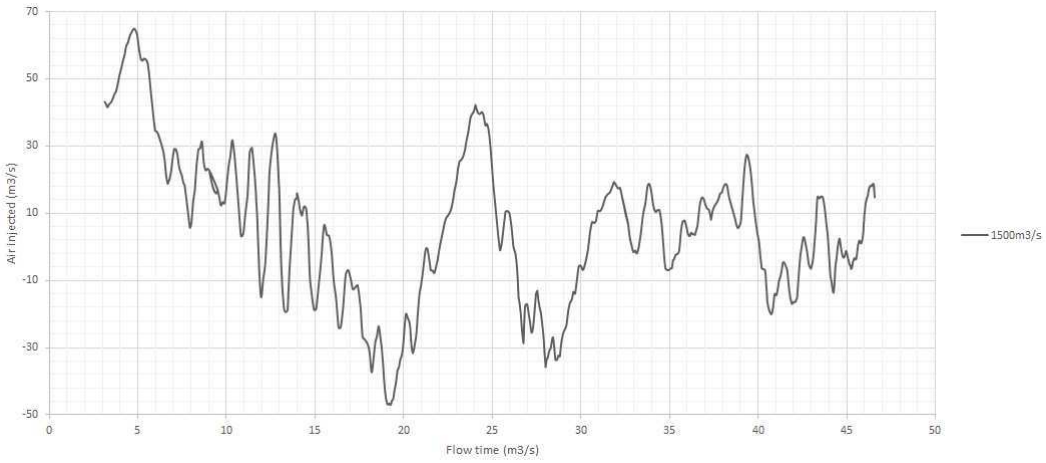

FIGURE 6.16: Air flow injected at the aerator in function of flow time (3D-1500m^3/s)

average air flow was 11.2m^3/s and it is consistent with the hypothesis mentioned above. There are some lead to understand and to improve the results :

- The spatial and temporal resolution are probably too large to capt this subtle phenomenon (the pressure depression is almost negligible in comparison with the other feature of the flow)
- Forcing the aeration in the beginning in order to trigger the aeration
- Place a surface in the middle of the shaft to avoid the surface turbulence at the top of the shaft and increase the precision of the record (there was an attempt to measure the air flow directly at the air vent but it failed)

It is difficult to estimate the expected air flow, as mentioned in the literature review there is some equations available based on the length of jet after the aerator and on the analysis of the geometry. However these equation are different for each geometry and contains terms not fulfill by our model (i.e Froude number above 5.4). Concerning the jet length the measure were not realized due to the last hypothesis.

The low air flow coupled with a relatively low Froude number and backflow effect in the aerator are indicator to study the eventuality of an aerator submergence.

On the 2D cross section we can easily identify some water in the reservoir and spray falling from the underside of the nappe, according to Chanson (1995) this behavior indicates the transition between a ventilated and filled cavity. We can observe the same comportment on the 3D cases with a lower resolution and a vague interface water-air. According to equation (2.6) the limit for the Froude number before filling is 3.57. This equation match well with the geometry of the aerator studied here that is why

FIGURE 6.17: Water in the aerator (2D-1500m^3/s)

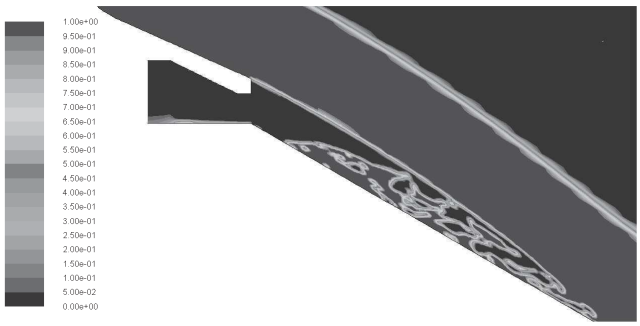

FIGURE 6.18: Spray falling from the underside of the nappe (2D-1900m^3/s)

it was preferred to the Chanson equation (2.5). The Froude number in the simulation range between [3.75;3.90] with a certain uncertainties on the water level surface and the velocity. These numbers are relatively close to the number presented by Shi in the equation (2.6).

Note that this paper does not imply that the aerators are close to the situation of submergence but only study this possibility in accord with the results obtained. One of conclusion drawn from the hypothesis would be that the aerators are in transition between the ventilation and submergence and that would explain the backflow effect and the relatively low air flow entrain by the chutes. Once again this hypothesis does not weight more than the others presented above.

6.2 Discussion and accuracy

In this part a numerical verification will be sketch and a discussion on accuracy, uncertainties and errors in CFD performed in order to estimate the validity of the work.

6.2.1 Verification of the model

The numerical verification procedure is based principally on convergence and comparison with calculated values, experimental data or measure. The convergence investigation involves iterative and grid convergence.

Iterative convergence Iterative convergence is said to be achieved with at least three orders of decrease magnitude in the normalized residuals for each equation solved. For transient problems, the convergence at each time step should be tested. The most

problematic residuals came from the continuity and x-velocity equation. While others achieved convergence very easily as it can be seen of Fig 6.19 the first one demand more iterations at each time step. To force iterative convergence it is possible to modify the under-relaxation factors but this option is only recommended for experience users. An other method, more flexible, was to increase the number of iteration (sometimes fixed to 100 iterations per time step) and in worst case stop the calculations before convergence at each time step.

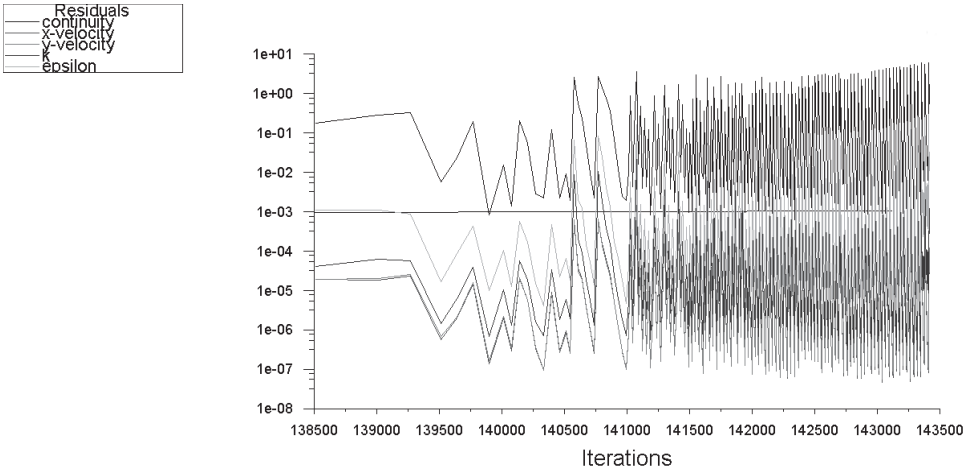

FIGURE 6.19: Iterative convergence (2D-1500m^3/s)

Grid convergence The examination of the spatial convergence is a method to estimate the dicretization error in a CFD simulation. The principle is to perform a simulation on two or more successively thinner mesh and compare the result with the coarser grid. If the output are roughly the same the discretization error is negligible and it is useless to refine the mesh. This study could not be performed as it is extremely time consuming. Some test were made in the 2D case between grid of 150 250 and 500 thousand cell on a short period and the result did not justify the utilization of such massive mesh. However in the 3D cases it is clear without grid refinement study to estimate that the results would be greatly improve (i.e interface between fluids).

The comparison with data available were in this case already performed in the results section.

6.2.2 Uncertainty and error in CFD simulations

The numerical solution are approximated solution which lead to several uncertainties and errors. The following classification gives an overview of the possible errors.

- Physical modeling errors
  A modeling error is the difference between the real flow and the exact solution of the model based on mathematical equations. All the simplification made to resolve the problem (i.e boundary conditions, empirical turbulence model, 2D, ...) in the sake of an efficient computation are a part of modeling errors.

- Discretization errors
  The discretization error is the difference between the exact solution of the differential equation and the exact solution of the approximated solutions. This error tends to zero when the grid spacing and time step come close zero.

- Iterative convergence error
  Iterative errors are the difference between the exact solution of the approximated equation and the solution obtained by the iterative process. As said before the convergence was difficult to achieve for some equations and probably lead to some inaccuracies.

- Usage Errors These errors are the least evident and are only controllable through training and experience of the users. Furthermore they can exist at every steps of the process (geometry, mesh, CFD, post-processing).

It was decided to present this list after the results to reassess them and put them in perspective with the probable errors.

Chapter 7

Conclusion

This project analyzed the air entrainment in spillways and the behavior of the flow in a stilling basin. There are still open question concerning the undervalued air entrainment and the backflow effect. It has already pointed out that the calculations were done on a laptop computer and therefore did not allow to refine the computational domain as it should have been necessary. Future works should use more computational power and calibrate the model by precise measure at key points of the spillway. Despite this it may be stated that some similarities were found concerning the surface water level in the basin and the velocity on the chute.

In the very beginning of the project it was decided to neglect the study of the reservoir in order to save some computational power. However an unsteady simulation of the flow in the basin coupled with the air entrainment remain an ambitious and challenging project. It would have been interesting to treat both of this conflicting subject in different simulation to have a better understanding of the phenomenon and reliable result.

Bibliography

[1] Falvey, H.T (1980) *"Air-Water Flow in Hydraulic Structures"* Bureau of Reclamation, Denver.

[2] Glazov, A.I. (1984) *"Calculation of the air-capturing ability of a flow behind an aerator ledge"* Hydrotechnical Construction Vol.18.

[3] ICOLD (1987) *"Spillways for dams"* B58 Commission Internationale des Grands Barrages, Paris.

[4] Chanson, H. (1989) *"Flow downstream of an aerator"* Journal of Hydraulic Research Vol.27, Paris.

[5] Falvey, H.T (1990) *"Cavitation in chutes and spillways"* Bureau of Reclamation, Denver.

[6] Rutschmann, P. and Hager,W.H. (1990) *"Air entrainment by spillway aerator"* Jl of Hyd. Engrg. Vol116.

[7] ICOLD (1992) *"Spillways. Shockwaves and air entrainment"* B81 Commission Internationale des Grands Barrages, Paris.

[8] Chanson, H. (1995) *"Predicting the filling of ventilated cavities behind spillway aerator"* Journal of Hydraulic Research Vol.33, Brisbane.

[9] Pope, S.B. (2000) *"Turbulent Flows"* Cambridge University Press, Cambridge.

[10] Gaskin, S. (2003) *"Air demand for a ramp-offset aerator as a function of spillway slope, ramp angle and Froude number"* McGill University, Montreal.

[11] Kramer, K. (2004) *"Development of aerated chute flow"* Swiss Federal Institute of Technology, Zurich.

[12] Cuong Nguyen, N. (2005) *"Turbulence Modelling"* Massachusetts Institute of Technology, Cambridge.

[13] ANSYS Fluent *"User's Guide 6.3"*.

[14] NASA *"NPARC Alliance CFD Verification and Validation Web Site "*.